Inorganica Chimica Acta xxx (2017) xxx–xxx

Contents lists available at ScienceDirect

Inorganica Chimica Acta

journal homepage: www.elsevier.com/locate/ica

Research paper

Preparation and characterization of myoglobin reconstituted with Fe(II) oxaporphyrin: The monoanionic macrocycle provides unique cyanide binding behavior for the ferrous species

Hiroyuki Meichin [a], Koji Oohora [a,b,c], Takashi Hayashi [a,*]

[a] Department of Applied Chemistry, Graduate School of Engineering, Osaka University, Suita 565-0871, Japan
[b] Frontier Research Base for Global Young Researchers, Graduate School of Engineering, Osaka University, Suita 565-0871, Japan
[c] PRESTO, Japan Science and Technology Agency (JST), Kawaguchi 332-0012, Japan

ARTICLE INFO

Article history:
Received 27 April 2017
Received in revised form 19 June 2017
Accepted 21 June 2017
Available online xxxx

This article is dedicated to Prof. Sóvágó

Keywords:
Reconstituted myoglobin
Monoanionic macrocycle
Iron oxaporphyrin
Cyanide binding

ABSTRACT

Iron-oxaporphyrin possessing two propionate side chains (**FeOP**) was synthesized as an artificial cofactor for myoglobin. The autoxidation of **FeOP** provides a ferric μ-oxo bridged diiron structure. The Fe^{II}/Fe^{III} redox potential of **FeOP** dimethyl ester in acetonitrile is +310 mV vs an Ag|AgCl electrode as determined by cyclic voltammetry. The value is positively shifted by 710 mV from that of the native heme cofactor, indicating that the ferrous species is stabilized in the oxaporphyrin framework. Myoglobin reconstituted with $\mathbf{Fe^{II}OP}$ was prepared in the presence of dithionite and characterized by UV–vis spectroscopy, ESI-TOF MS, and size exclusion chromatography. Interestingly, autoxidation of the reconstituted protein is found to release the cofactor from the heme pocket, suggesting that the affinity of $\mathbf{Fe^{III}OP}$ for the apoprotein is dramatically reduced. Furthermore, cyanide binds to $\mathbf{Fe^{II}OP}$ in the heme pocket of myoglobin with a binding constant of $1.2 \times 10^4\ M^{-1}$, although native deoxymyoglobin has no affinity for cyanide. These findings demonstrate that **FeOP** is a new type of artificial cofactor for myoglobin which provides a ferrous species with unique characteristics.

1. Introduction

Porphyrin, a macrocycle with 18 π-electrons, includes four pyrrole rings. Iron protoporphyrin IX complex, heme *b*, plays important roles in binding of small molecules such as O_2, NO and CO [1] as well as in enzymatic activities including biosynthesis of hormones [2], drug metabolism [3], and hypochlorite production [4]. These functions harness various redox states of the iron center. Other enzymes utilize different metal porphyrinoid compounds such as a nickel corphin complex (F430) and a cobalt corrinoid complex (cobalamin) (Fig. 1). F430 is used in the active site of methyl coenzyme M reductase, a methane-evolving enzyme of methanogenic archaea [5,6]. The corphin framework has monoanionic character which stabilizes a Ni(I) species as an active intermediate. Cobalamin is found in cobalamin-dependent enzymes such as diol dehydratase [7–9] and methionine synthase [10,11]. In methionine synthase, a specific Co(I) species is known to be involved in the catalytic cycle. The corrin framework of cobalamin also has monoanionic character.

Myoglobin (Mb), a ubiquitous mammalian oxygen storage hemoprotein, uses the heme cofactor which is also used in various oxidative heme enzymes such as cytochrome P450 and heme-containing peroxidases such as horseradish peroxidase. Over several decades, various efforts in the field of protein engineering have demonstrated enhancement of enzymatic activity of Mb as well as ligand binding affinities [12,13]. One of the methods used in these engineering efforts is reconstitution of Mb with its native heme molecule being substituted for an artificially-synthesized heme analogue [14–27]. Recently, our group has been focusing on reconstitution in efforts to modify the function of Mb. For instance, Mb reconstituted with iron porphycene, a constitutional isomer of iron porphyrin, dramatically enhances O_2 binding affinity. In addition, O_2/CO discrimination is reversed compared to native Mb [20]. Furthermore, manganese porphycene in the heme pocket of Mb has catalytic activity toward hydroxylation of inert alkanes [21]. Porphyrin analogues such as corrole and corrin derivative have also been found to have interesting influences as artificial cofactors for Mb [22–24]. For instance, an iron complex

* Corresponding author.
E-mail address: thayashi@chem.eng.osaka-u.ac.jp (T. Hayashi).

http://dx.doi.org/10.1016/j.ica.2017.06.054
0020-1693/

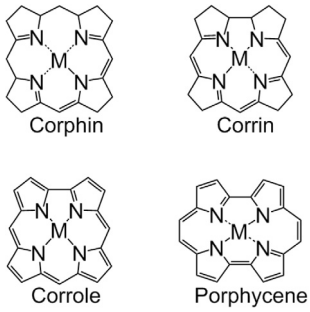

Fig. 1. Molecular structures of representative metal porphyrinoid complexes.

consisting of a corrole ring, which is a trianionic macrocycle, has been found to accelerate one-electron oxidation of a peroxidase substrate, relative to native Mb [22]. Moreover, a corrinoid framework as a monoanionic macrocycle forms a cobalt complex in Mb which promotes a reaction similar to that of cobalamin-dependent methionine synthase [23,24]. Recently, progress has also been made in incorporating porphyrins containing noble metals such as iridium and ruthenium into apoMb, and their activities have been tested [25–27]. We have conducted a series of studies of metal complexes of tetrapyrrole macrocycles to modulate the physicochemical properties and reactivities of the metal center. Another promising strategy toward development of unique artificial hemoproteins is represented by reconstitution with an artificial cofactor where one of the four pyrrolic nitrogen atoms is substituted with another heteroatom such as oxygen or sulfur. The O- and S-substituted porphyrins, which are known as oxaporphyrin and thiaporphyrin, respectively, provide the porphyrin with monoanionic character at the macrocycle core [28]. It is particularly interesting that these porphyrinoids stabilize a low-valent species of a coordinated metal in the framework [29,30]. Therefore, we have recently prepared an iron complex of oxaporphyrin with a furan ring instead of a pyrrole ring (Fig. 2). The present work describes preparation and physicochemical properties of a new water-soluble iron oxaporphyrin (**FeOP**) with two propionate side chains and Mb reconstituted with **FeOP** as an artificial cofactor.

2. Experimental

2.1. Instruments

UV–vis spectral measurements were carried out with a UV-2550 or UV-3150 double-beam spectrophotometer (Shimadzu) or V-670 UV–vis-NIR Spectrophotometer (JASCO). pH values were monitored using an F-52 pH meter (HORIBA). ESI-TOF MS analyses were performed on a micrOTOF-II mass spectrometer (Bruker). ^{1}H and ^{13}C NMR spectra were recorded on a DPX 400 or Avance III HD spectrometer (Bruker). Chemical shifts are reported in ppm relative to the internal TMS signal (0.00 ppm). Electrochemical studies were carried out using a potentiostat (CompactStat, Ivium Technologies) using a platinum wire as a counter electrode, an Ag|AgCl (saturated NaClaq: BAS) electrode as a reference and a polished platinum disk as a working electrode under anaerobic conditions. The detection of transiently formed species and kinetic measurements were conducted with a rapid scan stopped-flow system (Unisoku) constructed with a Xe source probe light. CD spectra were recorded at 25 °C on a J-820AC spectropolarimeter (JASCO). Air sensitive manipulations were performed in a UNILab glove box (MBRAUN).

2.2. Synthesis of ***FeOP***

All chemicals were purchased from Wako, TCI, Nacalai, and Sigma-Aldrich and used as received unless otherwise noted. Pyrrole derivatives **1**, **2** [22], **4** [31] and 1,4-diformylfuran **6** [32] were prepared according to reported procedures. **FeOP** was prepared as described below (Scheme 1).

2.2.1. Preparation of dipyrromethane ***3***

Pyrrole **1** (1.00 g, 2.68 mmol) and pyrrole **2** (0.91 g, 2.68 mmol) were dissolved in a mixture of glacial acetic acid (65 mL) and water (13 mL). To the solution, *p*-toluenesulfonic acid monohydrate (90 mg, 0.47 mmol) was added and the mixture was stirred for 24 h at ambient temperature. The reaction mixture was then poured into ice-water (300 mL) and carefully neutralized with sodium bicarbonate, followed by extraction with dichloromethane.

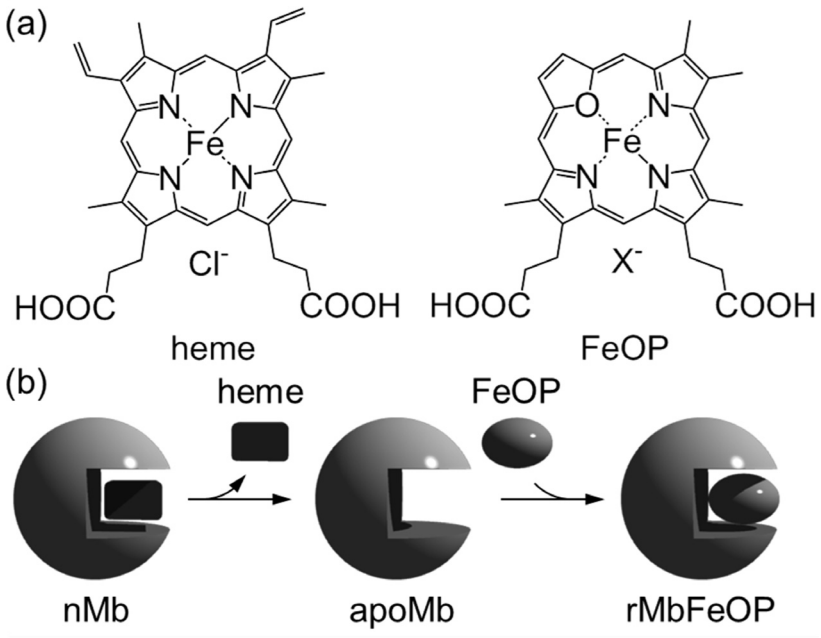

Fig. 2. (a) Molecular structures of heme and iron oxaporphyrin (**FeOP**) and (b) schematic representation of the reconstitution of myoglobin.

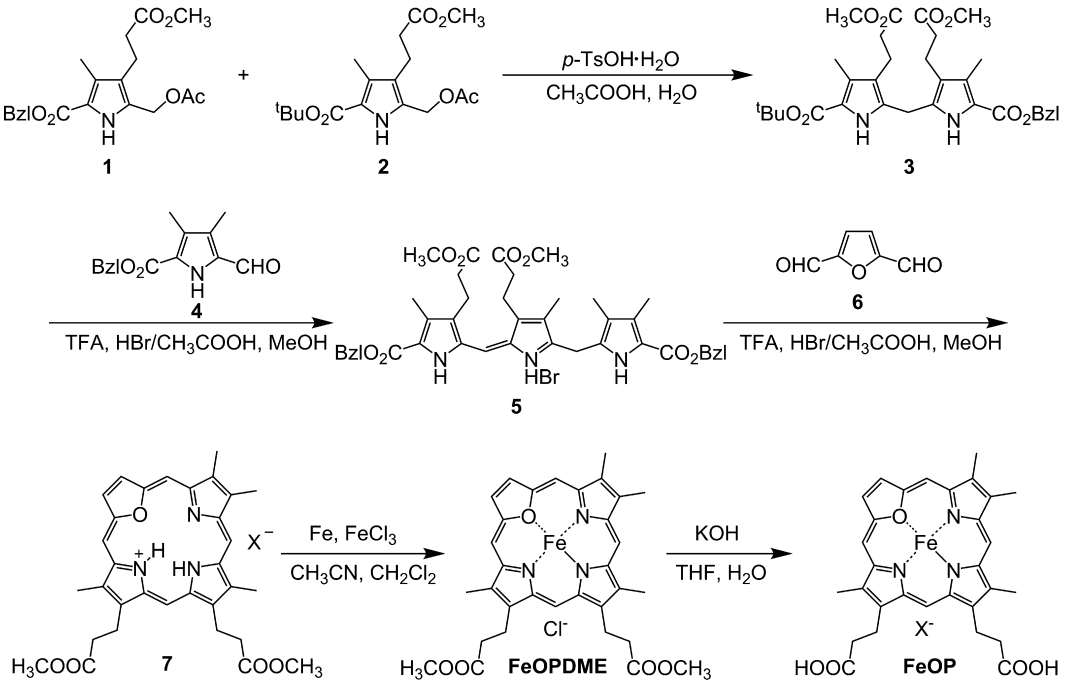

Scheme 1. Synthesis of **FeOP**.

After washing with saturated $NaHCO_{3aq}$ and brine, the organic phase was dried over Na_2SO_4 and dried using a rotary evaporator. The crude product was then purified by silica gel column chromatography (Hexane/AcOEt = 47/3–1/1) to afford pure product **3** (544 mg, 0.94 mmol, 35%). ^{1}H NMR (400 MHz, $CDCl_3$) δ = 10.0 (1H, s), 9.31 (1H, s), 7.17–7.09 (5H, m), 5.07 (2H, s), 3.84 (2H, s), 3.49 (3H, s), 3.43 (3H, s) 2.60 (4H, m), 2.25 (4H, m), 2.14 (3H, s), 2.10 (3H, s), 1.36 (9H, s) (Fig. S1). ^{13}C NMR (100 MHz, $CDCl_3$) δ = 173.49, 173.36, 161.53, 161.18, 136.22, 131.15, 129.59, 128.19, 128.19, 127.67, 127.55, 125.50, 120.05, 119.61, 119.19, 117.47, 79.94, 65.33, 60.13, 51.35, 34.43, 28.19, 22.43, 20.65, 19.15, 13.91, 10.54, 10.45 (Fig. S2). ESI-TOF MS (positive mode) calculated for $[M + Na]^+$, 603.268; found 603.272.

*2.2.2. Preparation of tripyrrin **5***

Dipyrromethane **3** (200 mg, 0.35 mmol) was dissolved in 4 mL of trifluoroacetic acid (TFA) under a nitrogen atmosphere and stirred for 5 min at ambient temperature. To this solution, formylpyrrole **4** (116 mg, 0.45 mmol) in 10 mL of methanol was added and the solution was further stirred for 90 min at ambient temperature. Then 30% HBr/AcOH (70 μL, 0.36 mmol) was added. The solution was then stirred for an additional 30 min before removal of the solvent on a rotary evaporator to provide a red crude oil **5** (381 mg). The obtained oil was then used in the next reaction without purification.

*2.2.3. Preparation of oxaporphyrin **7***

Crude tripyrrin **5** (330 mg) was stirred in a mixture of 30% HBr/AcOH (1.4 mL) and TFA (7 mL) for 6 h under a nitrogen atmosphere. The solution was diluted with 500 mL of methanol and then diformylfuran **6** (54 mg, 0.44 mmol) in 10 mL of methanol was added to this solution. Then the mixture was stirred for 12 h before removal of the solvent on a rotary evaporator. The obtained red oil was dissolved in dichloromethane and washed with brine three times. The organic phase was dried over Na_2SO_4, evaporated and purified by silica gel column chromatography ($CHCl_3$/CH_3-OH = 49/1–3/2) to afford oxaporphyrin **7** (32 mg, 0.059 mmol, 17% in two steps). ^{1}H NMR (400 MHz, $CDCl_3$) δ = 11.16 (1H, s), 10.82 (1H, s), 10.61 (1H, s), 10.45 (1H, s), 10.36 (1H, s), 10.08 (1H, s), 4.59–4.56 (2H, t, J = 6.4 Hz) 4.40–4.37 (2H, t, J = 7.2 Hz), 3.89 (3H, s), 3.63 (3H, s), 3.62 (3H, s), 3.59 (3H, s), 3.34–3.27 (4H, m), 1.25 (6H, s). ^{13}C NMR (100 MHz, $CDCl_3$) δ = 173.41, 52.06, 52.00, 36.52, 36.11, 29.85, 21.77, 21.70, 12.50, 12.30, 12.22, 12.04, 1.20, 0.14. ESI-TOF MS (positive mode) calculated for $[M + H]^+$, 540.249; found 540.250.

*2.2.4. Preparation of FeOP dimethyl ester (**FeOPDME**)*

To oxaporphyrin **7** (6.4 mg, 11.8 μmol) and iron powder (200 mg), degassed acetonitrile (20 mL), dichloromethane (20 mL), and $FeCl_3$ (23 mg, 142 μmol) were added under a nitrogen atmosphere. The solution was refluxed for 2 h and residual solid iron was filtered and followed by evaporation of solvent. The crude product was purified by gel filtration column chromatography in methanol to give **FeOPDME** (5.5 mg, 8.7 μmol, 74%). HR-ESI-TOF MS (positive mode) calculated for $[M–Cl]^+$, 594.1686; found 594.1690.

*2.2.5. Preparation of **FeOP***

FeOPDME (5.5 mg, 8.7 μmol) was dissolved in 1 mL of THF under a nitrogen atmosphere, and 1 mL of 0.05 M KOH solution was added. This mixture was stirred for 2 h at ambient temperature. The reaction mixture was carefully neutralized with 0.05 M HCl solution. After evaporation, the crude product was purified by gel filtration column chromatography in methanol to afford product **FeOP** (1.2 mg, 2.0 μmol, 23%). HR-ESI-TOF MS (positive mode) calculated for $[M–Cl]^+$, 566.1373; found 566.1361.

*2.3. Electrochemical measurement of **FeOPDME***

Cyclic voltammograms (CVs) were obtained in the potential range of −1.5 to 0.7 V (vs saturated Ag|AgCl reference electrode) at scan rate of 10 to 300 mV/s in degassed acetonitrile containing 5% DMF and 54 mM of tetrabutylammonium hexafluorophosphate as an electrolyte at 25 °C.

2.4. ^{1}H NMR analysis of **FeOPDME** using Evans method

The molar susceptibility of **FeOPDME** was determined using the Evans technique. ^{1}H NMR spectra of **FeOPDME** (2.5 mM) were measured in chloroform-d_1 solution containing dichloromethane as a reference. The equations below were used in the analysis (Eqs. (1)(3)).

$$\chi_M^{para}(m^3/mol) = 3 \times \Delta\delta \times 10^{-6}/(1000 \times M) \quad (1)$$

$$\mu_{eff} = \sqrt{\chi_M^{para} \times 3 \times k \times T/N_A \times \mu_0}/\mu_B \quad (2)$$

$$\mu_{eff} = g\sqrt{S(S+1)} \quad (3)$$

where $\Delta\delta$ is difference of chemical shift of CH_2Cl_2 in ppm in the presence and absence of **FeOPDME**, M is concentration of **FeOPDME** in mol/L, μ_{eff} is the magnetic susceptibility, k is the Boltzmann constant (1.38×10^{-23} (J/K)), T is temperature in K, N_A is the Avogadro constant ($6.02 \times 10^{23}(mol^{-1})$), μ_0 is the magnetic permeability of a vacuum ($4 \times \pi \times 10^{-7}(T^2m^3/J)$), μ_B is the Bohr magneton (9.27×10^{-24}(J/T)), and g is the g value for electron spin (2.002).

2.5. Preparation of rMb(**FeOP**)

Horse heart Mb was purchased from Sigma-Aldrich and purified by CM-Cellulose cation exchange column (Wako). Removal of the heme molecule from Mb was performed by the reported procedure [33]. An **Fe^{II}OP** solution (60 μL in total, 600 μM in 100 mM potassium phosphate buffer containing 16.7 mM sodium dithionite) was added dropwise to an apoMb solution (3 mL, 6 μM in 100 mM potassium phosphate buffer at pH 7.0) under a nitrogen atmosphere. Excess sodium dithionite and **FeOP** were removed by gel filtration chromatography using a HiTrap desalting column (5 mL, GE Healthcare) with 100 mM potassium phosphate buffer at pH 7.0 under anaerobic conditions. The obtained protein solution was stored anaerobically at 4 °C.

2.6. Oxidation of rMb(**Fe^{II}OP**) with potassium ferricyanide

To a solution of rMb(**Fe^{II}OP**) (400 μL, 450 μM in 100 mM potassium phosphate buffer at pH 7.0), a potassium ferricyanide solution (8.8 μL, 45 mM in 100 mM potassium phosphate buffer at pH 7.0) was added under nitrogen atmosphere. UV–vis and CD spectra were measured before and after addition of potassium ferricyanide.

2.7. Ligand binding studies of rMb(**Fe^{II}OP**)

To a freshly prepared rMb(**Fe^{II}OP**) solution in 100 mM potassium phosphate buffer at pH 7.0 (7.8 μM, 3 mL), potassium cyanide (30 μL, 7.8 mM in 100 mM potassium phosphate buffer at pH 7.0) was added anaerobically and UV–vis spectra were measured. The kinetics of cyanide binding were further studied under anaerobic conditions. The transient absorption spectra of the reaction of rMb(**Fe^{II}OP**) or aqua-met native myoglobin (nMb) (35 μM) with potassium cyanide (350–1050 μM) were monitored using a stopped-flow rapid scanning apparatus in 100 mM potassium phosphate buffer at pH 7.0 at 25 °C. The absorption changes were fitted to a single exponential equation to determine apparent rate constants k_{obs} at various concentrations of cyanide anion. The association rate constants k_{on}, dissociation constants k_{off}, and affinities for cyanide anion K_{CN}- were determined with plots of k_{obs} against concentration of cyanide anion. The concentrations of cyanide anion were determined by the following Henderson–Hasselbach equation (Eq. (4)).

$$pH = pK_a - \log\left(\frac{[HCN]}{[CN^-]}\right) = pK_a - \log\left(\frac{C_0 - [CN^-]}{[CN^-]}\right) \quad (4)$$

where pK_a is 9.2 [34] and C_0 is the concentration of added KCN.

3. Results and discussion

Despite the large number of known porphyrinoid compounds, reports on oxaporphyrin are quite limited [29,30,35–38]. In 1971, A. W. Johnson and coworkers reported the synthesis and properties of alkyl group-substituted oxaporphyrin as a monohydrobromide adduct. In this work, oxaporphyrin **7** was isolated in its protonated form. The protonation and deprotonation of the inner nitrogen atom are reversible upon addition of HCl_{aq} or $NaOH_{aq}$ to oxaporphyrin dissolved in methanol, as confirmed by UV–vis spectral changes in Fig. 3. This behavior is consistent with the report of Johnson et al. [35].

Insertion of iron into oxaporphyrin **7** was carried out in a similar fashion to generate a thiaporphyrin derivative [36]. The reaction was completed within 2 h to afford reddish brown compound (**FeOPDME**). The ESI-TOF mass spectrum of **FeOPDME** provides a peak at m/z = 594.169, which is consistent with the calculated exact mass number for $[M–Cl]^+$. This finding supports the formation of a ferrous species in the macrocycle with consideration of the monoanionic feature of the oxaporphyrin framework. This assignment was also confirmed by measurement of the molar

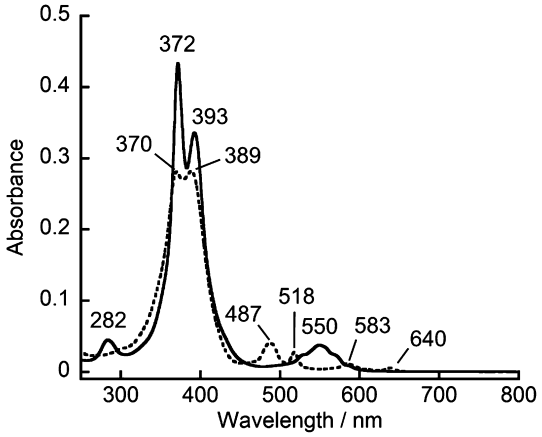

Fig. 3. UV–vis absorption spectra of oxaporphyrin **7** in methanol with 10 mM hydrochloric acid (solid line) and 50 mM sodium hydroxide (dotted line) containing 1% water at 25 °C.

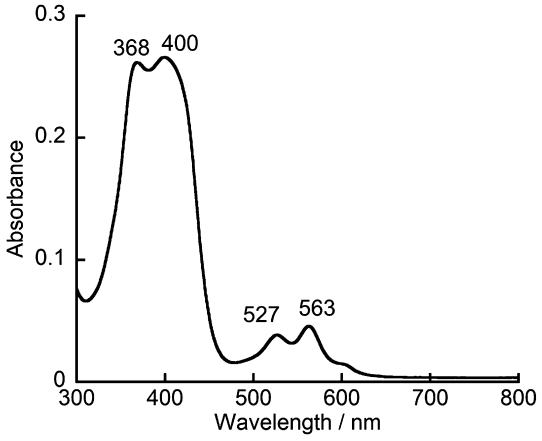

Fig. 4. UV–vis absorption spectrum of ferrous **FeOPDME** in methanol at 25 °C.

susceptibility of **FeOPDME** using the Evans method [39]. According to the difference of the chemical shift of reference dichloromethane in chloroform-d_1 (Fig. S5), the molar susceptibility was determined to be 1.25×10^{-7} m^3mol^{-1}, which is in agreement with a complex with $S = 2$. The UV–vis absorption spectrum of **Fe^{II}OPDME** is shown in Fig. 4. The characteristic split Soret band, two characteristic Q-bands and one shoulder-like Q-band are observed and these are mostly consistent with those of a previously reported iron complex of an oxaporphyrin derivative [37]. The CV measurements revealed two redox peaks at +0.31 V and −1.1 V vs Ag|AgCl in acetonitrile (Fig. S6). The former redox peak is assigned to the Fe^{II}/Fe^{III} process, which is positively shifted by 710 mV compared to that of heme *b*, indicating significant stabilization of the ferrous species in oxaporphyrin. The positive shift of the $E_{1/2}$ value of the Fe^{II}/Fe^{III} process in **FeOPDME** is similar to the observation made in the previous report of a TPP-type oxaporphyrin iron complex [37]. The latter redox peak is attributed to the formation of a one-electron reduced species of the macrocycle, because oxaporphyrin **7** has a reversible redox peak in the CV measurement at −1.1 V vs Ag|AgCl (Fig. S6).

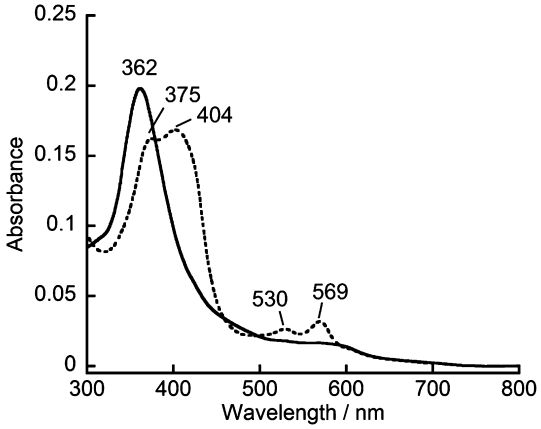

Fig. 5. UV–vis absorption spectra of the μ-oxo dimer of ferric state of **FeOP** (solid line) and monomer of the ferrous state of **FeOP** (dotted line) in methanol at 25 °C.

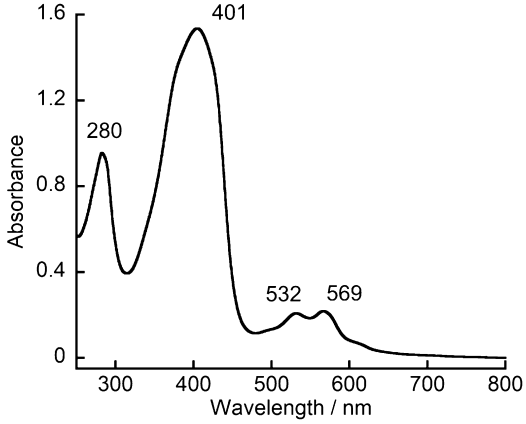

Fig. 6. UV–vis spectrum of rMb(**FeOP**) in 100 mM potassium phosphate buffer at pH 7.0 at 25 °C.

The methyl ester moieties were successfully hydrolyzed under basic conditions to yield **FeOP**. After the reaction, the split Soret band and the characteristic Q-bands disappear in the UV–vis spectrum (Fig. 5). This finding suggests that the ferrous state of iron oxaporphyrin is spontaneously oxidized to a ferric μ-oxo dimer product under aerobic conditions [37]. The ESI-TOF mass spectrum of the reaction mixture has a peak with $m/z = 574.1349$, in which the isotope pattern indicates $z = 2+$ (Fig. S7). This value is consistent with the calculated value of the ferric μ-oxo dimer complex ($m/z = 574.1356$ ($z = 2+$)). Interestingly, it was found that washing the ferric μ-oxo dimer complex in dichloromethane with 0.1 M HCl removes the iron ion with recovery of the oxaporphyrin free-base species. Instead of employing acidification, the monomeric ferrous state of **FeOP** complex was obtained by reduction of the μ-oxo dimer complex upon the addition of an excess amount of sodium dithionite. The formation of the ferrous species was confirmed by UV–vis spectroscopy (Fig. 5).

Next, insertion of the **Fe^{III}OP** μ-oxo dimer into the heme pocket of Mb was attempted after removal of heme. However, a UV–vis spectral change upon the addition of the dimer into the solution of the apoprotein was not observed because of the highly stable μ-oxo bridge structure. Thus, **Fe^{II}OP** was inserted into apoMb in the presence of sodium dithionite (Fig. 6). The titration curve in Fig. 6**a** clearly shows the curvature at a 1:1 ratio, indicating stoichiometric binding of **Fe^{II}OP** with apoMb. Size exclusion chromatography suggests that the elution volume monitored at 400 nm and 280 nm for the obtained reconstituted protein is consistent with that observed for the native protein (Fig. 7**b**). In addition, the ESI-TOF mass spectrum of the reconstituted protein indicated a 9+ ionized form (calcd: 1947.451, found: 1947.351) (Fig. S8), which confirms formation of rMb(**FeOP**).

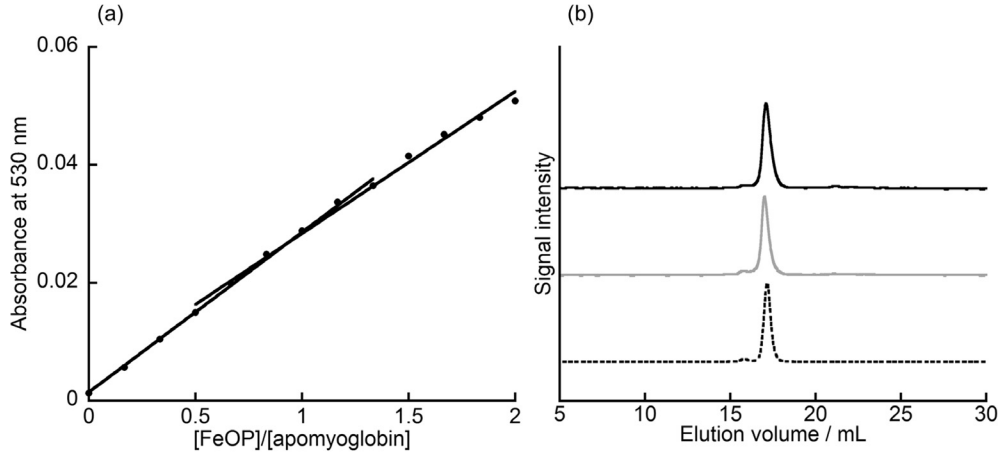

Fig. 7. (a) Plots of absorbance at 530 nm against the amount of added **Fe^{II}OP** and (b) size exclusion chromatogram of rMb(**FeOP**) (black solid line: 280 nm, gray solid line: 400 nm) and nMb (black dotted line: 409 nm) in 100 mM potassium phosphate buffer at pH 7.0 at 4 °C.

The autoxidation behavior of rMb(**Fe^{II}OP**) was studied. UV–vis spectral changes of rMb(**Fe^{II}OP**) were observed with clear isosbestic points after exposure to air (Fig. 8**a**) and characteristic Q-bands essentially disappear within 48 h. CD spectral changes (Fig. 8**b**) suggest that **FeOP** is released from the heme pocket of Mb, because the Cotton effect in the Soret region, which is derived from the chiral environment of the heme pocket, obviously decreases after the reaction. In contrast, the UV–vis spectrum of rMb(**Fe^{II}OP**) under a nitrogen atmosphere does not show any changes over 12 h (Fig. S9), supporting our assumption that the spectral changes observed under aerobic conditions are derived from the autoxidation. Furthermore, the disappearance of the CD signal in the Soret region after the addition of potassium ferricyanide indicates that **Fe^{III}OP** is released from the Mb matrix (Fig. 9). Despite a lot of researches on engineering of Mb, artificial metal complex cofactors which possess dicationic charge are quite limited. [23] It is proposed that the dicationic charged complex **Fe^{III}OP** significantly decreases in the affinity for the Mb matrix because the hydrophobic interaction between native heme and Mb matrix accounts for the factor of 10^5–10^7 M^{-1} in the overall binding affinity of 1×10^{14} M^{-1}. [40] Similarly, oxidation of ferrous heme to ferric state in soluble guanylyl cyclase, a hemoenzyme, results in release of heme from protein matrix due to lack of hydrophobic interaction [41].

A study of ligand binding to rMb(**Fe^{II}OP**) was conducted. The addition of potassium cyanide to freshly prepared rMb(**Fe^{II}OP**) induces a color change from brown to pink. UV–vis spectral changes are observed with clear isosbestic points, indicating that cyanide is capable of binding to the iron center of **Fe^{II}OP** (Fig. 10) with a binding constant of 1.2×10^4 M^{-1}, although native

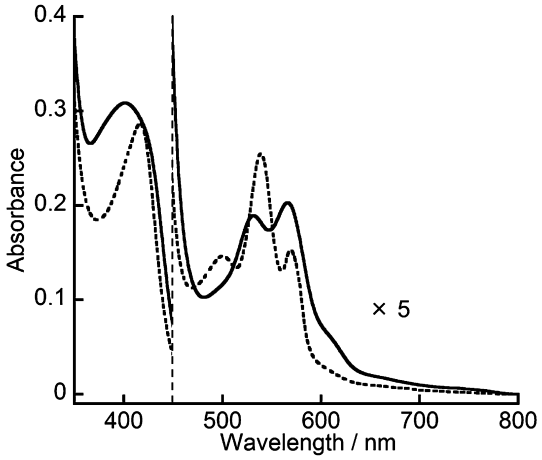

Fig. 10. UV–vis spectrum of 7.8 μM of rMb(**Fe^{II}OP**) in the absence (solid line) and presence (dotted line) of potassium cyanide in 100 mM potassium phosphate buffer at pH 7.0 containing 10 mM sodium dithionite at 25 °C. [rMb(**Fe^{II}OP**)] = 7.8 μM. [KCN] = 770 μM.

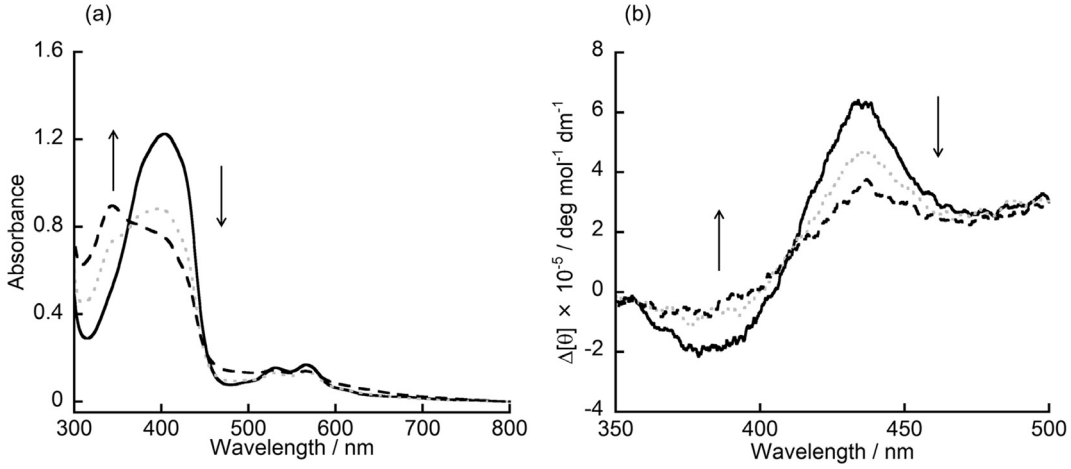

Fig. 8. (a) UV–vis and (b) CD spectral changes of rMb(**FeOP**) over 48 h under aerobic conditions in 100 mM potassium phosphate buffer at pH 7.0 at 25 °C.

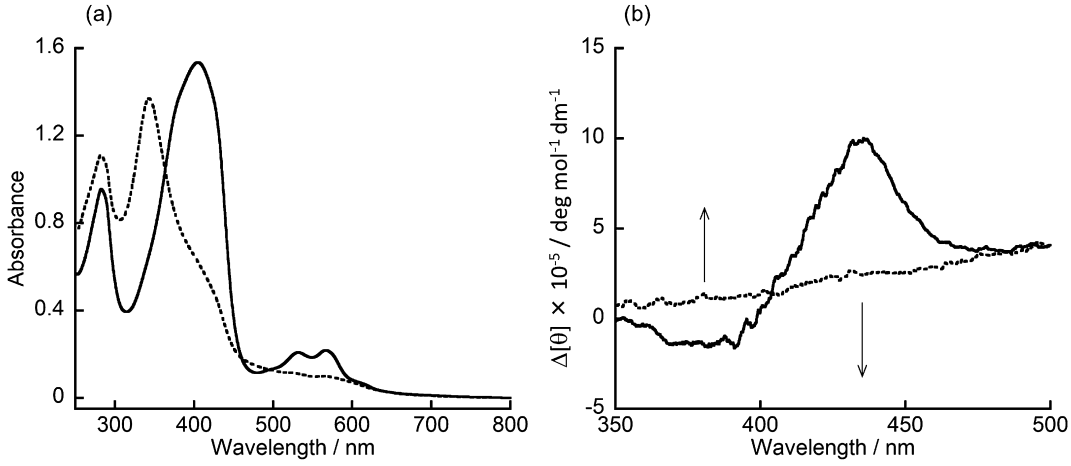

Fig. 9. (a) UV–vis and (b) CD spectra of rMb(**FeOP**) in the absence (solid line) and presence (dotted line) of potassium ferricyanide under anaerobic conditions in 100 mM potassium phosphate buffer at pH 7.0 at 25 °C. [rMb(**FeOP**)] = 441 μM. [$K_3Fe(CN)_6$] = 860 μM.

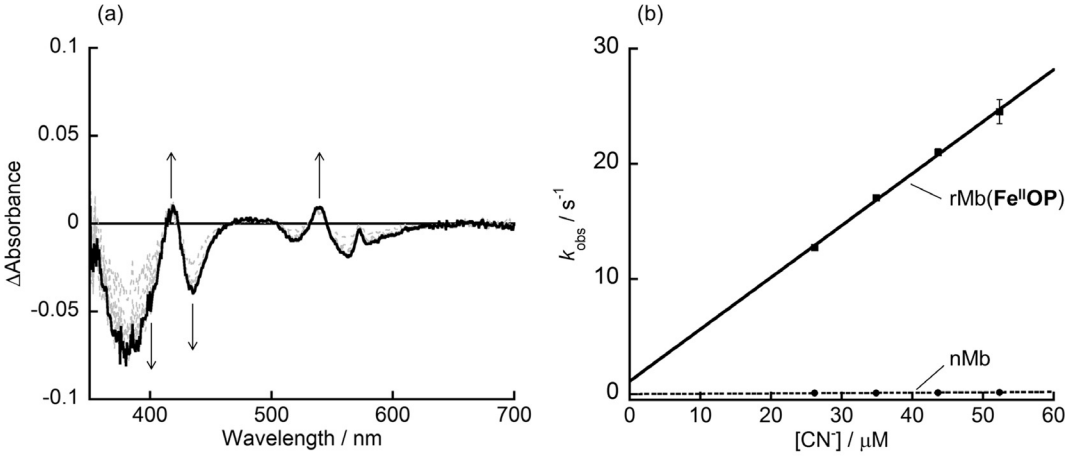

Fig. 11. (a) Differential transient absorption changes of rMb(**Fe^{II}OP**) during the reaction with potassium cyanide. Spectra were measured every 0.05 s over 0.5 s (solid line: 0 s) and (b) plots of rate constants for the reaction of potassium cyanide with (solid line) rMb(**Fe^{II}OP**) and (dotted line) nMb against various concentrations of cyanide ion in 100 mM potassium phosphate buffer at pH 7.0 at 25 °C. In the case of rMb(**FeOP**), the solution contained 10 mM sodium dithionite.

Table 1
Cyanide Binding Parameters for Native and Reconstituted Mb.

Protein	k_{on} ($\mu M^{-1}\ s^{-1}$)[a]	k_{off} (s^{-1})[b]	K_{CN-} (μM^{-1})
ferric nMb	$8.9 \pm 0.3 \times 10^{-5}$	8.0×10^{-4} [d,e]	0.11
ferrous rMb(FeOP)[c]	$1.3 \pm 0.1 \times 10^{-2}$	1.1 ± 0.6[b]	$1.2 \pm 0.6 \times 10^{-2}$

Reaction conditions: 100 mM phosphate buffer (pH 7.0) at 25 °C.
[a] Association rate constants of cyanide ligand.
[b] Dissociation rate constants of cyanide ligand.
[c] in 100 mM potassium phosphate buffer containing 10 mM sodium dithionite.
[d] in 110 mM sodium phosphate buffer at pH 6.6 at 25 °C, protein concentration of 5.2 μM.
[e] Ref [42].

deoxymyoglobin does not interact with cyanide. Transient absorption spectra were obtained using stopped-flow techniques with various concentrations of potassium cyanide (Fig. 11). Apparent association and dissociation rate constants, k_{on} and k_{off}, were determined as summarized in Table 1. The association of cyanide with rMb(**Fe^{II}OP**) is relatively fast with a k_{on} value of $1.3 \times 10^{-2}\ \mu M^{-1}\ s^{-1}$, which is 150-fold faster than that of ferric nMb. One of the possible reasons for the faster binding may be attributed to the different position of the iron atom in the porphyrinoid plane of **Fe^{II}OP,** relative to its position in heme *b* [20]. The iron atom in **Fe^{II}OP** could be located in the porphyrinoid plane without any deviation from the plane according to the previous report [43,44], whereas the iron atom in heme *b* is out of plane (with a distance of $\Delta_{Mb} = 0.29$ Å from the protoheme plane) [45]. In contrast, the affinity of cyanide for rMb(**Fe^{II}OP**) is 9-fold lower than that of ferric nMb due to its fast dissociation rate. An X-ray crystal structure analysis and/or theoretical study will be needed to further understand the interesting ligand binding behavior of rMb(**Fe^{II}OP**).

4. Conclusion

This work is the first example of the use of iron oxaporphyrin (**FeOP**) as a new myoglobin cofactor. The precursor **FeOPDME** provides a positively shifted Fe^{II}/Fe^{III} redox potential compared to that of heme, indicating that the oxaporphyrin framework clearly stabilizes the ferrous species. The cofactor, **Fe^{II}OP**, was then successfully incorporated into apoMb to form the reconstituted protein in the presence of dithionite. **Fe^{II}OP** is stable and remains in the protein pocket under a nitrogen atmosphere at room temperature for over 12 h, whereas under aerobic conditions rMb(**Fe^{II}OP**) releases **FeOP** from the heme pocket via autoxidation. Furthermore, rMb(**Fe^{II}OP**) is capable of binding cyanide as an axial ligand, which is sharply different from nMb. These findings suggest that a metal oxaporphyrin complex has potential for providing new functions as an artificial cofactor of hemoproteins. Characterization of the structure and enzymatic activity of rMb(**Fe^{II}OP**) is now in progress.

Acknowledgements

This work was supported by Grants-in-Aid for Scientific Research provided by JSPS KAKENHI Grant Numbers JP15H05804, JP24655051, JP15H00944, JP22105013, and JP16H00837, and JST PRESTO (JPMJPR15S2). H.M. acknowledges support from the Program for Leading Graduate Schools for Osaka University: Interdisciplinary Program for Biomedical Sciences (IPBS).

Appendix A. Supplementary data

Supplementary data associated with this article can be found, in the online version, at http://dx.doi.org/10.1016/j.ica.2017.06.054.

References

[1] A. Ghosh, The Smallest Biomolecules: Diatomics and their Interactions with Heme Proteins, Elsevier, 2008. pp. 3–17.
[2] B. Meunier, S.P. de Visser, S. Shaik, Chem. Rev. 104 (2004) 3947–3980.
[3] U.M. Zanger, M. Schwab, Pharmacol. Ther. 138 (2013) 103–141.
[4] S.J. Klebanoff, J. Leukoc. Biol. 77 (2005) 598–625.
[5] D. Ankel-Fuchs, R.K. Thauer, Eur. J. Biochem. 156 (1986) 171–177.
[6] M. Goubeaud, G. Schreiner, R.K. Thauer, Eur. J. Biochem. 243 (1997) 110–114.
[7] B. Kräutler, A. Sigel, Metal Ions in Life Science, Springer, 2009. pp. 1–51.
[8] K. Gruber, B. Puffer, B. Kräutler, Chem. Soc. Rev. 40 (2011) 4346–4363.
[9] K.L. Brown, Chem. Rev. 105 (2005) 2075–2150.
[10] C.L. Drennan, S. Huang, J.T. Drummond, R.G. Matthews, M.L. Lidwig, Science 266 (1994) 1669–1674.
[11] R.G. Matthews, Acc. Chem. Res. 34 (2001) 681–689.
[12] B.A. Springer, S.G. Sligar, J.S. Olson, G.N. Jr, Phillips, Chem. Rev. 94 (1994) 699–714.
[13] F. Draghi, A.E. Miele, C. Travaglini-Allocatelli, B. Vallone, M. Brunori, Q.H. Gibson, J.S. Olson, J. Biol. Chem. 277 (2002) 7509–7519.
[14] H. Sato, T. Hayashi, T. Ando, Y. Hisaeda, T. Ueno, Y. Watanabe, J. Am. Chem. Soc. 126 (2004) 436–437.
[15] S. Chakraborty, J. Reed, M. Ross, M.J. Nilges, I.D. Petrik, S. Ghosh, S. Hammes-Schiffer, J.T. Sage, Y. Zhang, C.E. Schulz, Y. Lu, Angew. Chem. Int. Ed. 53 (2014) 2417–2421.
[16] M. Bröring, F. Brégier, O. Burghaus, C. Kleeberg, Z. Anorg, Allg. Chem. 636 (2010) 1760–1766.
[17] M. Bordeaux, V. Tyagi, R. Fasan, Angew. Chem. Int. Ed. 54 (2015) 1744–1748.
[18] T. Hayashi, Y. Hitomi, H. Ogoshi, J. Am. Chem. Soc. 120 (1998) 4910–4915.
[19] I. Hamachi, S. Shinkai, Eur. J. Org. Chem. 1999 (1999) 539–549.
[20] T. Matsuo, H. Dejima, S. Hirota, D. Murata, H. Sato, T. Ikegami, H. Hori, Y. Hisaeda, T. Hayashi, J. Am. Chem. Soc. 126 (2004) 16007–16017.

[21] K. Oohora, Y. Kihira, E. Mizohata, T. Inoue, T. Hayashi, J. Am. Chem. Soc. 135 (2013) 17282–17285.
[22] T. Matsuo, A. Hayashi, M. Abe, T. Matsuda, Y. Hisaeda, T. Hayashi, J. Am. Chem. Soc. 131 (2009) 15124–15125.
[23] T. Hayashi, Y. Morita, E. Mizohata, K. Oohora, J. Ohbayashi, T. Inoue, Y. Hisaeda, Chem. Commun. 50 (2014) 12560–12563.
[24] Y. Morita, K. Oohora, A. Sawada, K. Doitomi, J. Ohbayashi, T. Kamachi, K. Yoshizawa, Y. Hisaeda, T. Hayashi, Dalton Trans. 45 (2016) 3277–3284.
[25] H.M. Key, P. Dydio, D.S. Clark, J.F. Hartwig, Nature 534 (2016) 534–537.
[26] M.W. Wolf, D.A. Vargas, N. Lehnert, Inorg. Chem. 56 (2017) 5623–5635.
[27] G. Sreenilayam, E.J. Moore, V. Steck, R. Fasan, Adv. Synth. Catal. 359 (2017) 2076–2089.
[28] T. Chatterjee, V.S. Shetti, R. Sharma, M. Ravikanth, Chem. Rev. 117 (2017) 3254–3328.
[29] P.J. Chmielewski, L. Latos-Grażyński, M.M. Olmstead, A.L. Balch, Chem. Eur. J. 3 (1997) 268–278.
[30] E. Pacholska, P.J. Chmielewski, L. Latos-Grażyński, Inorg. Chim. Acta 273 (1998) 184–190.
[31] A.R. Battersby, M.G. Baker, H.A. Broadbent, C.J.R. Fookes, F.J. Leeper, J. Chem. Soc. Perkin Trans. 1 (1987) 2027–2048.
[32] D.W. Yoon, D.E. Gross, V.M. Lynch, J.L. Sessler, B.P. Hay, C.H. Lee, Angew. Chem. Int. Ed. 47 (2008) 5038–5042.
[33] F.W.J. Teale, Biochem. Biophys. Acta 35 (1959) 543.
[34] R.M. Izatt, J.J. Christensen, R.T. Pack, R. Bench, Inorg. Chem. 1 (1962) 828–831.
[35] M.J. Broadhurst, R. Grigg, A.W. Johnson, J. Chem. Soc. C (1971) 3681–3690.
[36] L. Latos-Grażyński, J. Lisowski, M.M. Olmstead, A.L. Balch, Inorg. Chem. 28 (1989) 1183–1188.
[37] M. Pawlicki, L. Latos-Grażyński, Inorg. Chem. 41 (2002) 5866–5873.
[38] S. Stute, L. Götzke, D. Meyer, M.L. Merroun, P. Rapta, O. Kataeva, W. Seichter, K. Gloe, L. Dunsch, K. Gloe, Inorg. Chem. 52 (2013) 1515–1524.
[39] I. Bertini, C. Luchinat, P. Turano, G. Battaini, L. Casella, Chem. Eur. J. 9 (2003) 2316–2322.
[40] M.S. Hargrove, D. Barrick, J.S. Olson, Biochemistry 35 (1996) 11293–11299.
[41] B.G. Fritz, X. Hu, J.L. Brailey, R.E. Berry, F.A. Walker, W.R. Montfort, Biochemistry 50 (2011) 5813–5815.
[42] R.P. Cox, M.R. Hollaway, Eur. J. Biochem. 74 (1977) 575–587.
[43] In ferric heme b, spin density exists in $d_{x^2-y^2}$ orbital of iron atom and this causes overlap between 2p-orbitals of pyrrole nitrogen atoms. The electron in $d_{x^2-y^2}$ orbital is accommodated in σ^* orbital to weaken the Fe–nitrogen bond, resulted in the out-of-plane position of iron in heme b. Latos-Grażyński et al. proposed unoccupied $d_{x^2-y^2}$ orbital for bisaryl adduct of Fe(II) oxaporphyrin complex. As a result, the iron atom is in the plane of oxaporphyrin.
[44] M. Pawlicki, L. Latos-Grażyński, Inorg. Chem. 43 (2004) 5564–5571.
[45] G.S. Kachalova, A.N. Popov, H.D. Bartunik, Science 284 (1999) 473–476.

Please cite this article in press as: H. Meichin et al., Inorg. Chim. Acta (2017), http://dx.doi.org/10.1016/j.ica.2017.06.054